Supplementary Information (SI) for Chemical Science.
This journal is © The Royal Society of Chemistry 2024

Electronic Supporting Information

A Comprehensive Approach for Elucidating the Interplay Between $4f^{n+1}$ and $4f^n5d^1$ Configurations in Ln^{2+} Systems

Maria J. Beltran-Leiva,[1] William Moore,[2] Tener F. Jenkins,[2] William J Evans,[2*] Cristian Celis-Barros[3*], Thomas E. Albrecht[4*]

[1]*Theoretical Division, Los Alamos National Laboratory, Los Alamos, New Mexico 87545, United States*

[2]*Department of Chemistry, University of California, Irvine, California 92697-2025, United States*

[3]*Radioisotope Science and Technology Division, Oak Ridge National Laboratory, Oak Ridge, TN 37830, USA*

[4]*Department of Chemistry and Nuclear Science & Engineering Center, Colorado School of Mines, Golden, Colorado 80401, United States*

*To whom correspondence should be addressed.

Table of Contents

Computational Details **3**

Geometry optimization and theoretical model 3

Multireference calculations 3

Ligand Field DFT calculations 7

Figures

Figure S1. Estimated Ln^{3+}/Ln^{2+} reduction potentials (V vs SHE)……....11

Figure S2. $4f^{n+1}$ to $4f^{n}5d^{1}$ promotion energies for the Ln^{2+} free ions reported by Dorenbos…… 12

Figure S1 Ground state electron densities of the $LnCp'_3$ complexes…… 13

Figure S2. Ground state electron densities of the $[LnCp'_3]^-$ complexes……14

Figure S5. Depiction of the *f*-orbitals……..15

Tables

Table S1 Multiplicities and number of roots employed in the CASSCF calculations of Ln^{3+} free ions and $LnCp'_3$ complexes. 8

Table S2 Multiplicities and number of roots employed in the CASSCF calculations of the $[LnCp'_3]^-$ complexes. 9

Table S3. $4f^{n+1} \rightarrow 4f^{n}5d^{1}$ promotion energies for the active spaces explored in this work.9

Table S4. Occupation of the CASSCF spin-free natural orbitals for Ce^{3+}, $CeCp'_3$ and $[CeCp'_3]^-$……...10

Table S5. Estimated quadrupole moments (Q_2) for divalent and trivalent lanthanide ions……14

Computational Details

Geometry optimization and theoretical model: The experimental coordinates of $LnCp'_3$ and $[LnCp'_3]^-$ (Ln = La, Ce, Pr, Nd, Sm, Eu, Gd, Tb, Dy, Ho, Er, Tm and Yb) complexes were obtained from cif files reported in the work of McDonald[1,2] and Fieser.[3] These coordinates were subjected to geometry optimizations in ADF version 2019,[4] with no symmetry or geometry constraints. Initially, the level of theory consisted of the generalized gradient approximation (GGA) Perdew-Burke-Ernzerhof (PBE) functional[5] with Slater-type basis functions (STO) triple-ζ plus polarization (TZP) without frozen-core.[6] These optimized coordinates were further employed for a second optimization process using the M06-2X functional,[7] as meta-hybrid functionals have proven accurate in modeling divalent lanthanide systems.[1–3,8–10] The relativistic effects were incorporated through the zeroth-order regular approximation (ZORA) of the Dirac equation.[11] Finally, analytical frequency calculations were performed on the optimized structures to confirm them as true minima.

Since these optimized structures are being subjected to expensive *ab initio* wavefunction calculations, the $SiMe_3$ groups were replaced with hydrogen atoms (Figure 1). According to initial explorations and a report by Fleischauer *et al.*,[12] the truncation of the complexes only affects the intensity of some bands. However, it does not significantly affect the position of the electronic states nor the nature of the excitations (Table S3).

Multireference calculations: Both $LnCp_3$ and $[LnCp_3]^-$ complexes along with the Ln^{2+} and Ln^{3+} free ions were subjected to *ab initio* wavefunction calculations using the OpenMolcas software.[13] In a first step, Hartree-Fock (HF) densities were calculated to serve as starting point for the multiconfigurational calculations. The metal center as well as C and H atoms

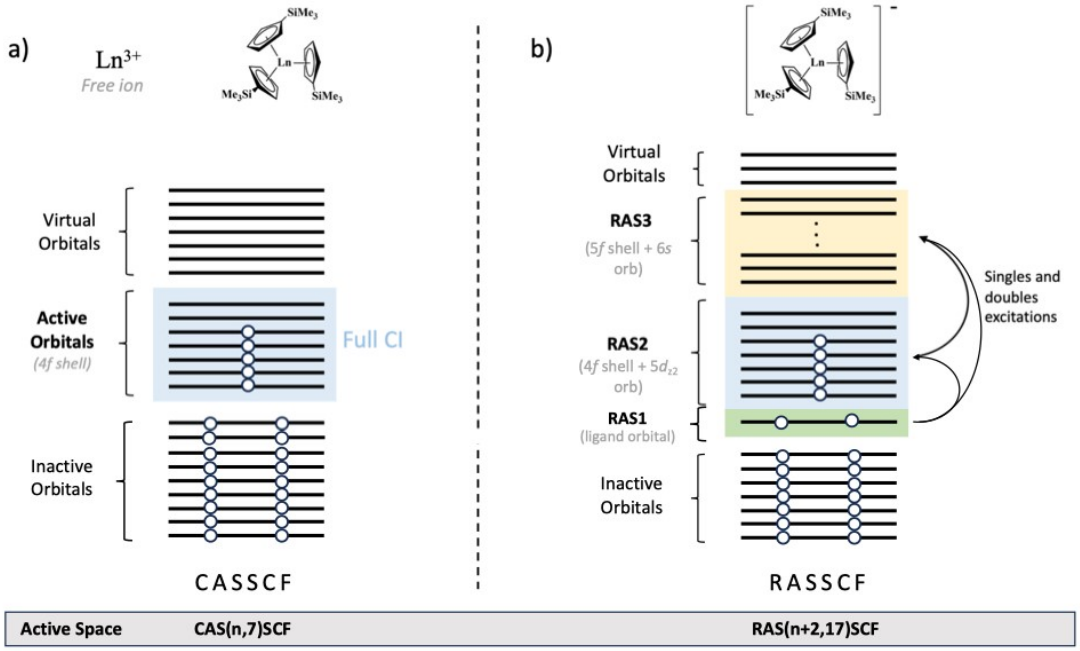

Figure S01. Active spaces employed for the Ln^{3+} free ions, $LnCp'_3$ complexes (a) and their reduced $[LnCp'_3]^-$ analogs (b).

were described thorough all-electron ANO-RCC Gaussian-type basis sets contracted to TZP quality.[14] Relativistic effects were incorporated through the 2-component Douglas-Kroll-Hess (DKH2) Hamiltonian.[15] To account for the static correlation present in lanthanide systems, the resulting wavefunctions for the Ln^{3+} free ions and $LnCp_3$ systems were employed as input for complete active space self-consistent field (CASSCF) calculations.[16] In case of the $[LnCp_3]^-$ complexes, the restricted active space self-consistent field (RASSCF) was employed instead.[17] The dynamic correlation was recovered through the multiconfigurational pair-density functional theory (MC-pDFT) method using the tPBE on-top functional.[18] In a final step, the spin-orbit coupling (SOC) was included via state interactions between the CASSCF/RASSCF wavefunctions through the restricted active space state interaction (RASSI) method.[19] The detail of the

multiplicities and number of roots employed for each lanthanide is shown in Table S1. The definition of the active spaces is explained in Figure S01.

Ln^{3+} and $LnCp_3$ complexes: In these cases, we are only interested in the composition of the ground state. Therefore, a minimum active space consisting of n electrons in seven 4*f* orbitals, CAS(n,7) was employed (Figure S02a). In case of the free ions, the keyword SUPSYM was employed to get atomic orbitals with pure spherical symmetry.

Ln^{3+} with and without spherical symmetry: Given the absence of a ligand field, in the free ions the *f* orbitals are degenerate. Therefore, after a regular SA-CASSCF where no spherical symmetry was imposed, a mixture of atomic orbitals is observed which is contrary to what we expect for a free atom (Figure S02). Additionally, the GS occupations (not the state average) are not consistent with what we expect from the Hund's rule that states the following: *"For a determined multiplicity, the term with the largest value of the total orbital angular momentum quantum number L has the lowest energy".* This is presumable due to the lack of spherical symmetry during the CASSCF procedure. Thus, we employed the SUPSYM keyword to restrict the orbital mixing between the atomic orbitals, which led to pure *f* orbitals (Figure S03) and orbital occupations that maximize the orbital angular momentum.

Ln^{2+} and $[LnCp_3]^-$ systems: In case of these reduced free-ions and complexes, we want to elucidate the nature of the ground state ($4f^{n+1}$ or $4f^n5d^1$) but also predict accurately the excited states to be able to calculate the $4f^{n+1}$ to $4f^n5d^1$ promotion energies. Given the sensitivity of divalent lanthanide systems to the treatment of the electronic correlation, we chose the active space following the guidelines presented by Barandiaran and Seijo in

2013.[20] These authors analyzed the $SrCl_2$:Yb^{2+} material and demonstrated that the inclusion of a second *f* shell into the active space improves the prediction of the promotion energies, especially for lanthanides having more than half-filled *f* shells. Since we successfully tested this strategy on Sm(II) crown complexes,[21] we incorporated the second *f* shell across the entire series to keep consistency. In addition to the 4*f*/5*f* shells, the $5d_{z2}$ and 6*s* orbitals were also included since hybridization between them was observed. Finally, a bonding ligand orbital exhibiting the appropriate symmetry to interact with the $f_{y(y2-3x2)}$ orbital was also included. Therefore, the active space for the $[LnCp_3]^-$ systems consisted of n + 2 electrons (n = 4*f* electrons) in 17 orbitals (4*f* shell + 5*f* shell + $5d_{z2}$ orb + 6*s* orb + ligand orb). To prevent orbitals from rotating out of the active space the SUPSYM keyword was employed. The decision of including the $5d_{z2}$ orbital instead of the entire 5*d* shell in the active space was primarily based on its differential stabilization relative to the other orbitals due to the pseudo-trigonal symmetry imposed by the Cp_3 coordination environment (see Figure 4). However, there is a previous report validating this theoretical approach.[22] Further discussion on the selection of the active spaces is given below (Results section).

<u>*Ground state electron densities*</u>: In order to plot the charge distributions of the studied systems for the Hund's rule ground state in their largest Mj state, the resulting spin-orbit-coupled states from the RASSI calculation were considered.[23] We specifically employed the keyword SONO which generates the natural spin orbitals containing the electron density of the specified spin-orbit states.[23] Then, the SOOrb.1 file associated to the first spin-orbit state was used as input for the GRID_IT module, where the plots were generated.

Ligand Field DFT calculations: This approach was considered to obtain the $4f^{n+1}$ to $4f^{n}5d^{1}$ promotion energies corresponding to the Ln^{3+} free ions. The calculations were performed using the ADF package version 2019.[4] The level of theory consisted of the PBE functional with Grimme corrections in its D3 formulation to account for the dispersion forces along with TZP basis sets for all the elements.[24] The relativistic effects were incorporated through the ZORA Hamiltonian. The multiplet manifolds of each Ln were calculated by diagonalizing the matrix elements of the LFDFT Hamiltonian.

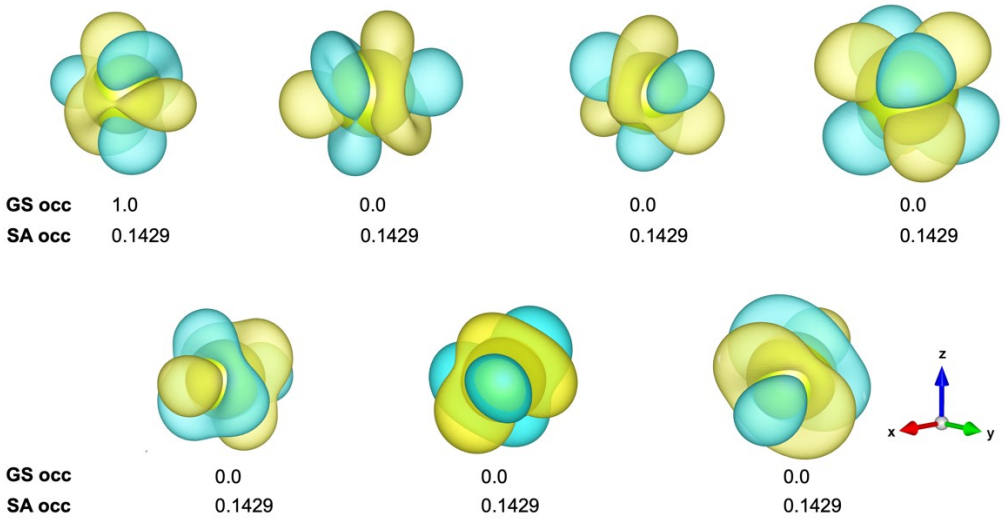

Figure S02. Depiction of GS *f*-orbitals resulting from a CAS(1,7)SCF calculation without spherical symmetry on Ce^{3+}. Isovalue=0.03

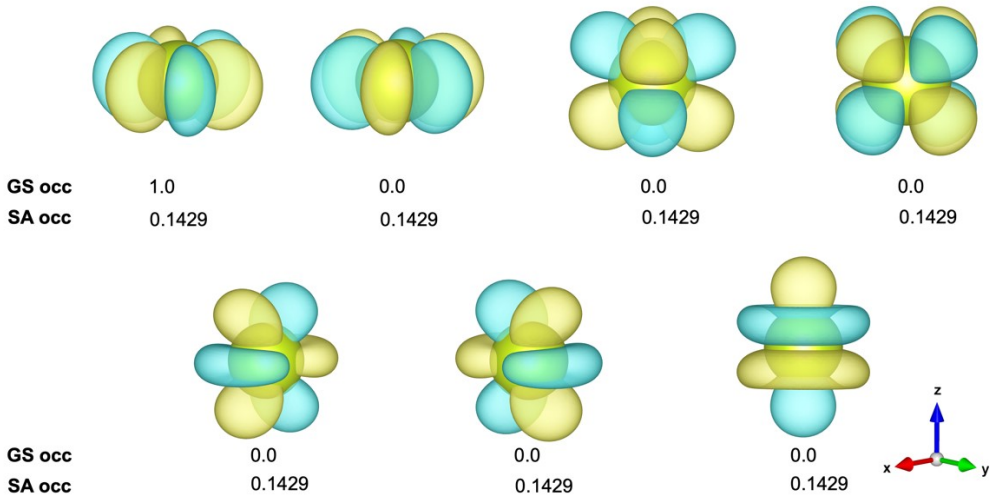

Figure S03. Depiction of GS *f*-orbitals resulting from a CAS(1,7)SCF calculation with spherical symmetry on Ce^{3+}. Isovalue=0.03

Table S01 Multiplicities and number of roots employed in the CASSCF calculations of Ln^{3+} free ions and $LnCp_3$ complexes.

Ln	Multiplicity (2S+1)							
	1	**2**	**3**	**4**	**5**	**6**	**7**	**8**
Ce	-	7	-	-	-	-	-	-
Pr	28	-	21	-	-	-	-	-
Nd	-	112	-	35	-	-	-	-
Sm	-	490	-	224	-	21	-	-
Eu	490	-	588	-	140	-	7	-
Gd	-	-	-	392	-	48	-	1
Tb	-	-	588	-	140	-	7	-
Dy	-	490	-	224	-	21	-	-
Ho	196	-	210	-	35	-	-	-
Er	-	112	-	35	-	-	-	-
Tm	28	-	21	-	-	-	-	-
Yb	-	7	-	-	-	-	-	-

Table S02 Multiplicities and number of roots employed in the CASSCF calculations of the Ln^{2+} free ions and $[LnCp_3]^-$ complexes.

Ln	Multiplicity (2S+1)								
	1	**2**	**3**	**4**	**5**	**6**	**7**	**8**	**9**
Ce	100	-	120	-	-	-	-	-	-
Pr	-	200	-	300	-	-	-	-	-
Nd	120	-	200	-	300	-	-	-	-
Sm	-	-	120	-	200	-	300	-	-
Eu	-	-	-	120	-	200	-	300	-
Gd	-	-	-	-	120	-	200	-	200
Tb	-	-	-	120	-	200	-	300	-
Dy	-	-	120	-	200	-	300	-	-
Ho	-	100	-	200	-	200	-	-	-
Er	100	-	200	-	300	-	-	-	-
Tm	-	200	-	300	-	-	-	-	-
Yb	100	-	120	-	-	-	-	-	-

Results

Structural parameters: Good agreement is observed between the optimized structures and the experimental data. The average Ln–Centroid (cnt) distances were predicted with errors of less than 1.2%, in the range 0.03 and 0.001 Å for the [LnCp'$_3$] complexes while for the divalent systems the error was in the range of 0.001 and 0.02 Å.

Average Ln-Cnt bondlengths for [LnCp'$_3$] and [LnCp'$_3$]$^-$ complexes					
System	**Experiment**	**Theory**	**System**	**Experiment**	**Theory**
$LaCp_3$	2.559	2.592	$[LaCp_3]^-$	2.586	2.609
$CeCp_3$	2.529	2.531	$[CeCp_3]^-$	2.558	2.542
$PrCp_3$	2.508	2.509	$[PrCp_3]^-$	2.535	2.526
$NdCp_3$	2.488	2.489	$[NdCp_3]^-$	2.519	2.537
$SmCp_3$	2.461	2.476	$[SmCp_3]^-$	2.608	2.600
$EuCp_3$	2.451	2.456	$[EuCp_3]^-$	2.607	2.603
$GdCp_3$	2.437	2.449	$[GdCp_3]^-$	2.468	2.489
$TbCp_3$	2.423	2.428	$[TbCp_3]^-$	2.446	2.439
$DyCp_3$	2.407	2.411	$[DyCp_3]^-$	2.443	2.432
$HoCp_3$	2.394	2.397	$[HoCp_3]^-$	2.426	2.418
$ErCp_3$	2.385	2.392	$[ErCp_3]^-$	2.416	2.409
$TmCp_3$	2.379	2.388	$[TmCp_3]^-$	2.502	2.501
$YbCp_3$	2.365	2.381	$[YbCp_3]^-$	2.508	2.496

Active space for [LnCp$_3$]$^-$ systems: Due to the availability of experimental data, the [EuCp$_3$]$^-$ complex was initially employed to define the active space to calculate the $4f^{n+1} \rightarrow 4f^n5d^1$ promotion energies. The active space selections were further tested in the [TmCp$_3$]$^-$ complex to analyze their performance when dealing with a more than half-filled

4*f* shell (Table S3). The promotion energies calculated for the free ions were taken as a reference to guide our analysis on the complexes.

Active Space #1: Our first natural approach was to include the 4*f* shell plus the $5d_{z2}$ orbital (RAS2) in the active space. This choice was rationalized given the non-bonding nature of these orbitals added to the more stabilized nature of the $5d_{z2}$ orbital with respect to the rest of the *d* shell. However, this approach led to significant deviations in the prediction of the promotion energies, with errors in the range of 7,000 – 10,000 cm^{-1} with respect to the experimental value in case of the $[EuCp_3]^-$ complex, and excessively large values in case of the $[TmCp_3]^-$ system.

Active Space #2: Our second attempt consisted in expanding the previous active space by adding a bonding ligand orbital that displays the appropriate symmetry to interact with the $f_{y(y2-3x2)}$ orbital (RAS1). Although some improvement was observed in the calculated promotion energies for $[EuCp_3]^-$, unrealistic values were obtained in case of the $[TmCp_3]^-$ system.

Active Space #3: Our final attempt considered an expansion of active space #2 by adding a second *f*-shell. This idea was based on the work of Barandiaran and Seijo,[20] where it is demonstrated that the incorporation of the 5*f* orbitals in the active space, increased the accuracy in the calculation of the promotion energies, due to a better treatment of the correlation effects. Although the system analyzed by these authors correspond to the highly symmetric $SrCl_2:Yb^{2+}$ material where D_{2h} symmetry was imposed, the conclusion remain valid for our less symmetric systems. Therefore, given the consistency observed

between Eu and Tm compounds, we decided to use this active space across the lanthanide series to calculate the $4f^{n+1} \rightarrow 4f^{n}5d^{1}$ promotion energies.

Table S3. $4f^{n+1} \rightarrow 4f^{n}5d^{1}$ promotion energies for the active spaces explored in this work. Negative values indicate the wrong GS configuration.

		$TmCp_3$		**$EuCp_3$**		**$EuCp'_3$***	
		cm^{-1}	**eV**	**cm^{-1}**	**eV**	**cm^{-1}**	**eV**
Active Space #1	RAS(n,8)	-109,700	-13.6	-13,827	-1.7	-14,795	-1.8
	RAS(n,8)-pDFT	-61,453	-7.6	-8,033	-1	-9,530	-1.2
	RAS(n,8)-pT2	115,963	14.3	16,820	2.1	18,119	2.2
	SO-RAS(n,8)	-112,304	-13.9	-17,179	-2.1	-18,071	-2.2
	SO-RAS(n,8)-pDFT	-65,069	-8.1	-10,280	-1.3	-11,671	-1.4
	SO-RAS(n,8)-pT2	112,706	13.9	15,179	1.9	16,394	2
Active Space #2	RAS(n+2,9)	-51,935	-6.5	23,022	2.9	3,463	0.4
	RAS(n+2,9)-pDFT	32,846	4	28,391	3.5	9,770	1.2
	RAS(n+2,9)-pT2	19,470	-2.4	16,597	2	13,292	1.7
	SO-RAS(n+2,9)	-52,797	-6.5	21,171	2.6	3,002	0.4
	SO-RAS(n+2,9)-pDFT	36,436	4.5	22,863	2.8	8,653	1.1
	SO-RAS(n+2,9)-pT2	20,930	2.6	15,760	1.9	12,122	1.5
Active Space #3	RAS(n+2,17)	-12,831	-1.6	21,297	2.9	15,190	1.9
	RAS(n+2,17)-pDFT	13,146	1.2	23,031	3.6	22,295	2.8
	RAS(n+2,17)-pT2	15,188	1.3	25,132	3.4	24,922	3.1
	SO-RAS(n+2,17)	-10,673	-1.7	19,991	2.5	13,854	1.7
	SO-RAS(n+2,17)-pDFT	11,890	1.3	21,014	2.6	20,897	2.6
	SO-RAS(n+2,17)-pT2	15,913	2.0	24,037	3	23,222	2.9

***The entire structure was employed for the calculation

Table S4. Occupation of the CASSCF spin-free natural orbitals for Ce^{3+}, $CeCp'_3$ and $[CeCp'_3]^-$ where J is the total angular momentum and M_J corresponds to the projections of J.

Ln	f_{3-}	f_{2-}	f_{1-}	f_0	f_{1+}	f_{2+}	f_{3+}	d_0
Ce^{3+}	0	0	0	0	0	0	1	0
$CeCp'_3$	0	0	0	0	1	0	0	0
$[CeCp'_3]^-$	0	0	0.01	0	0.01	0	0.99	0.99
Pr^{3+}	0.38	0.38	0.02	0.00	0.02	0.60	0.60	0
$PrCp'_3$	0.01	0.32	0.66	0	0.66	0.32	0.01	0
$[PrCp'_3]^-$	0.00	0.11	0.11	0.77	0.11	0.11	0.79	1.00
Nd^{3+}	0.16	0.16	0.28	0.28	0.66	0.66	0.78	0
$NdCp'_3$	0.21	0.21	0.79	0.00	0.79	0.09	0.91	0
$[NdCp'_3]^-$	0.00	0.21	0.79	0.08	0.79	0.20	0.92	1
Sm^{3+}	0.62	0.40	0.98	1.00	0.98	0.40	0.62	0
$SmCp'_3$	0.38	1.00	1.00	0.62	1.00	0.38	0.62	0
$[SmCp'_3]^-$	0.01	0.99	0.99	1.00	0.99	0.99	0.99	0
Eu^{3+}	0	1	1	1	1	1	1	0
$EuCp'_3$	0	1	1	1	1	1	1	0
$[EuCp'_3]^-$	1	1	1	1	1	1	1	0
Gd^{3+}	1	1	1	1	1	1	1	0
$GdCp'_3$	1	1	1	1	1	1	1	0
$[GdCp'_3]^-$	1	1	1	1	1	1	1	1
Tb^{3+}	1	1	1	1	1	1	2	0
$TbCp'_3$	1	1	1	1	2	1	1	0
$[TbCp'_3]^-$	1	1	1	1	1	1	2	1
Dy^{3+}	1.38	1.38	1.02	1	1.02	1.60	1.60	0
$DyCp'_3$	1.02	1.35	1.64	1.02	1.64	1.35	1.00	0
$[DyCp'_3]^-$	1.42	1.57	1.00	1.00	1.00	1.42	1.57	1
Ho^{3+}	1.16	1.16	1.28	1.28	1.66	1.66	1.78	0
$HoCp'_3$	1.21	1.21	1.79	1.09	1.79	1.00	1.91	0
$[HoCp'_3]^-$	1.38	1.52	1.47	1.03	1.50	1.48	1.59	1
Er^{3+}	1.22	1.34	1.34	1.72	1.72	1.84	1.84	0
$ErCp'_3$	1.19	1.72	1.98	1.13	1.88	1.28	1.82	0
$[ErCp'_3]^-$	1.09	1.91	1.22	1.74	1.26	1.78	2.00	1
Tm^{3+}	1.40	1.40	1.98	2.00	1.98	1.62	1.62	0
$TmCp'_3$	1.43	1.58	2	1.58	2	1.43	2	0
$[TmCp'_3]^-$	1	2	2	2	2	2	2	0
Yb^{3+}	1	2	2	2	2	2	2	0
$YbCp'_3$	1	2	2	2	2	2	2	0
$[YbCp'_3]^-$	2	2	2	2	2	2	2	0

Table S5. Estimated quadrupole moments (Q_2) for divalent and trivalent lanthanide ions.

	Q_2 (Ln^{3+})	Q_2 (Ln^{2+})	ΔQ_2	Observation
Ce	-0.626	-0.855	0.228	Remains oblate and high anisotropy
Pr	-0.613	-0.304	-0.309	Remains oblate but decreases in anisotropy
Nd	-0.232	0.262	0.030	Turns prolate with similar anisotropy
Sm	0.388	-	-	Turns spherical
Eu		0.000	-	Remains spherical
Gd	0.000	-0.717	0.717	Turns oblate with high anisotropy
Tb	-0.580	-0.611	0.031	Remains oblate with high anisotropy
Dy	-0.568	-0.234	-0.334	Remains oblate with decreased anisotropy
Ho	-0.222	0.224	0.002	Turns prolate with similar anisotropy
Er	0.218	0.538	0.321	Remains proplate with increased anisotropy
Tm	0.534	0.517	-0.017	Remains prolate with high anisotropy
Yb	0.522	0.000	-0.522	Turns spherical

$4f^{n+1}$
Crossover
$4f^{n}5d^{1}$

*Q_2 values were calculated based on equation $Q_2 = \alpha_J \langle r^2 \rangle_{4f} (2J^2 - J)$ using radial values (Angstroms) from reference 25 for Ln^{3+} and 10% radial increase for Ln^{2+} ions.

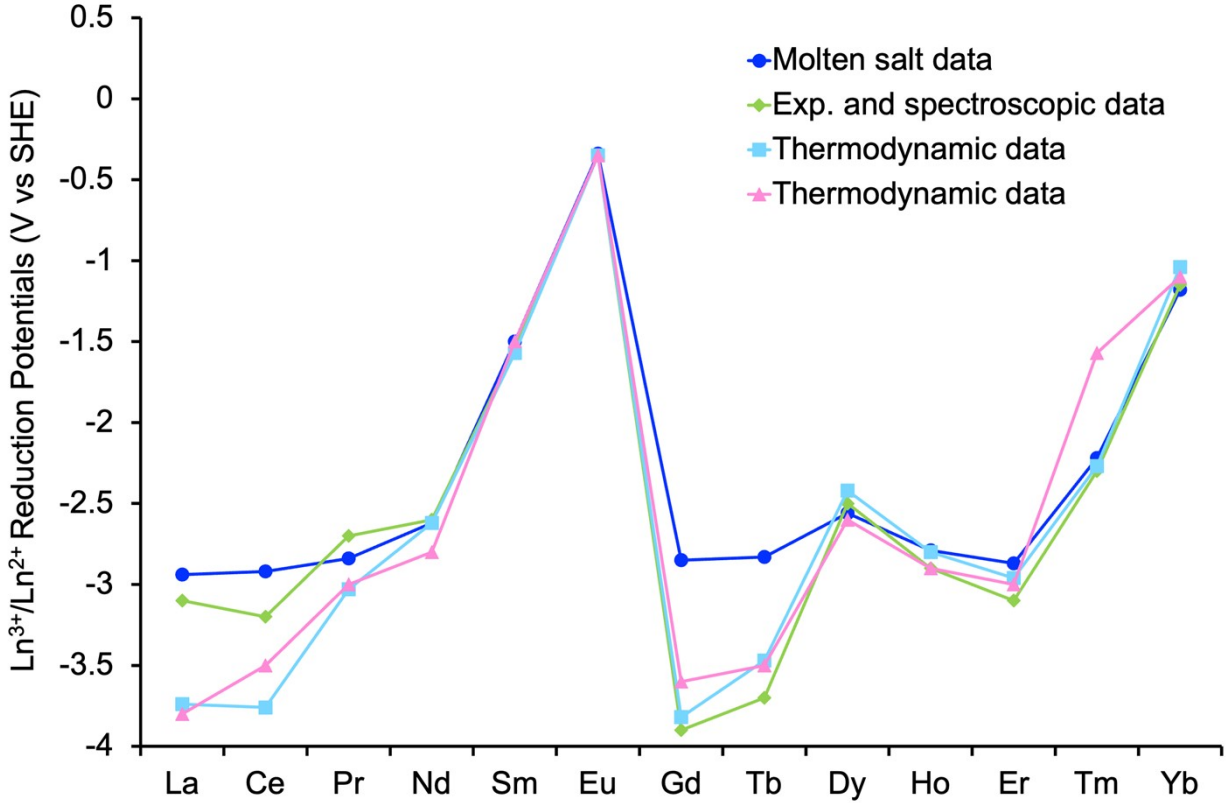

Figure S1. Estimated Ln^{3+}/Ln^{2+} reduction potentials (V vs SHE) based on experimental and spectroscopic data,[26,27] thermodynamic[28–33] and molten salt data[29–33].

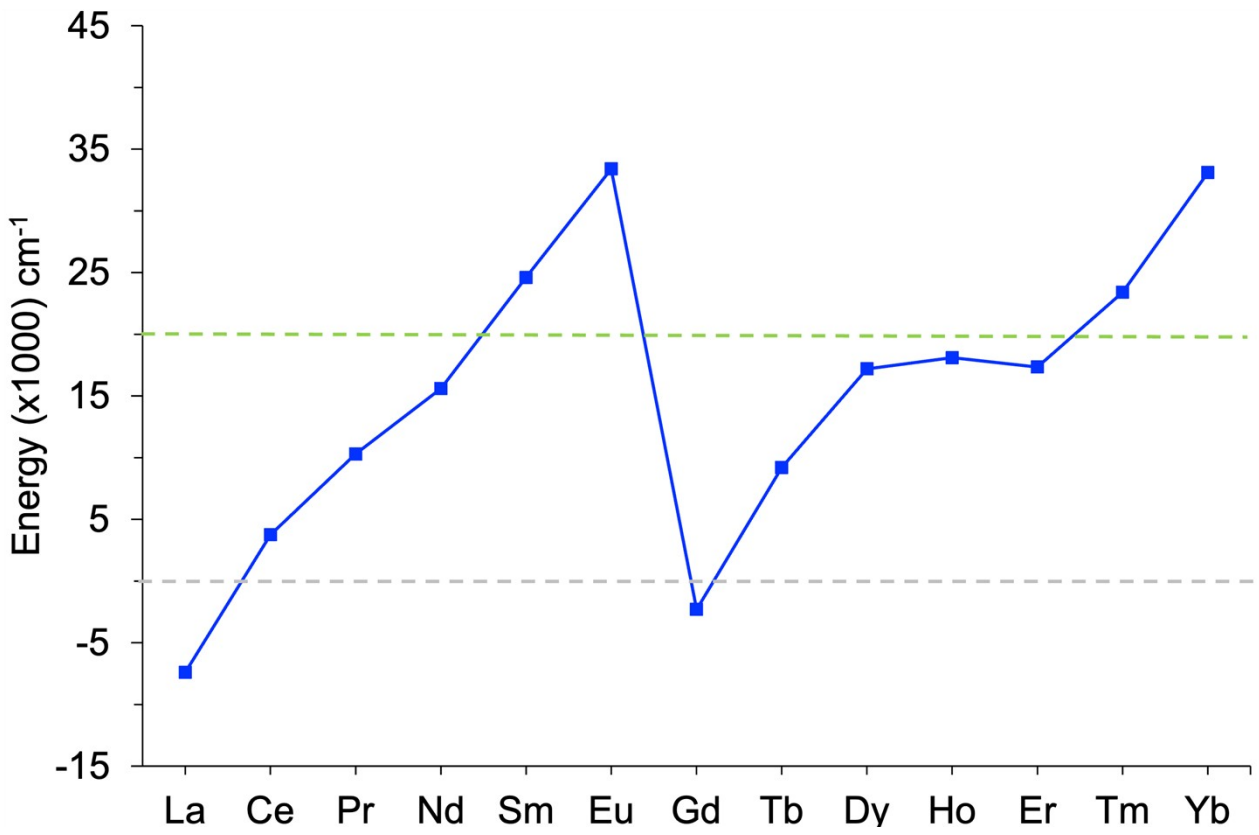

Figure S2. $4f^{n+1}$ to $4f^{n}5d^{1}$ promotion energies for the Ln^{2+} free ions reported by Dorenbos.[34] The gray dashed line indicates that for the free ions just La^{2+} and Gd^{2+} have a $4f^{n}5d^{1}$ configuration. The green dashed line indicates the shift in energy provided by the pseudo-trigonal Cp' chemical environment. The energy shift provided is *ca.* 20000 cm^{-1} allowing some Ln^{2+} afford the $4f^{n}5d^{1}$ configuration as a ground state.

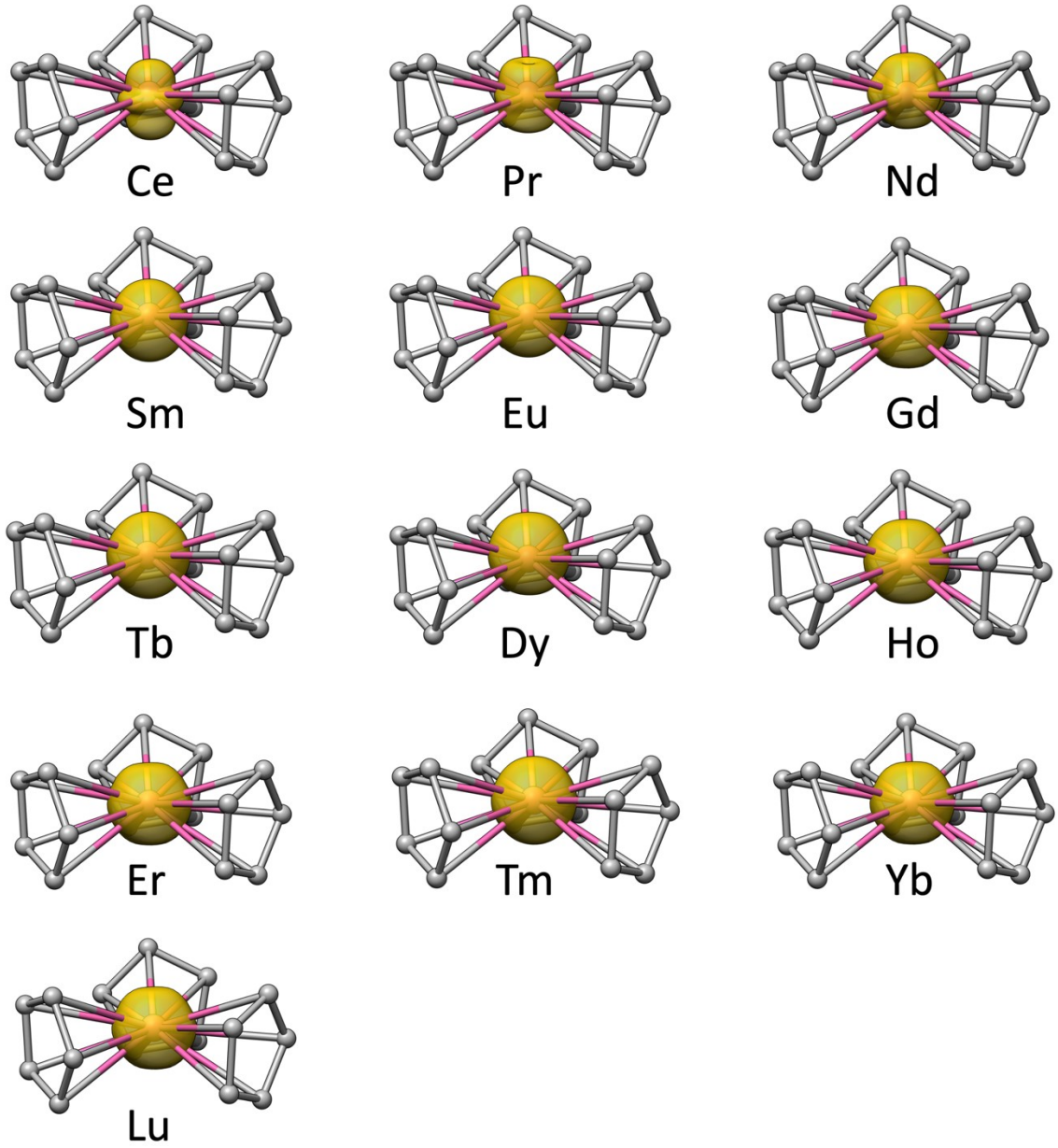

Figure S3 Ground state electron densities of the $LnCp_3$ complexes. This representation only considers the occupation numbers of the 4*f* natural spin orbitals.

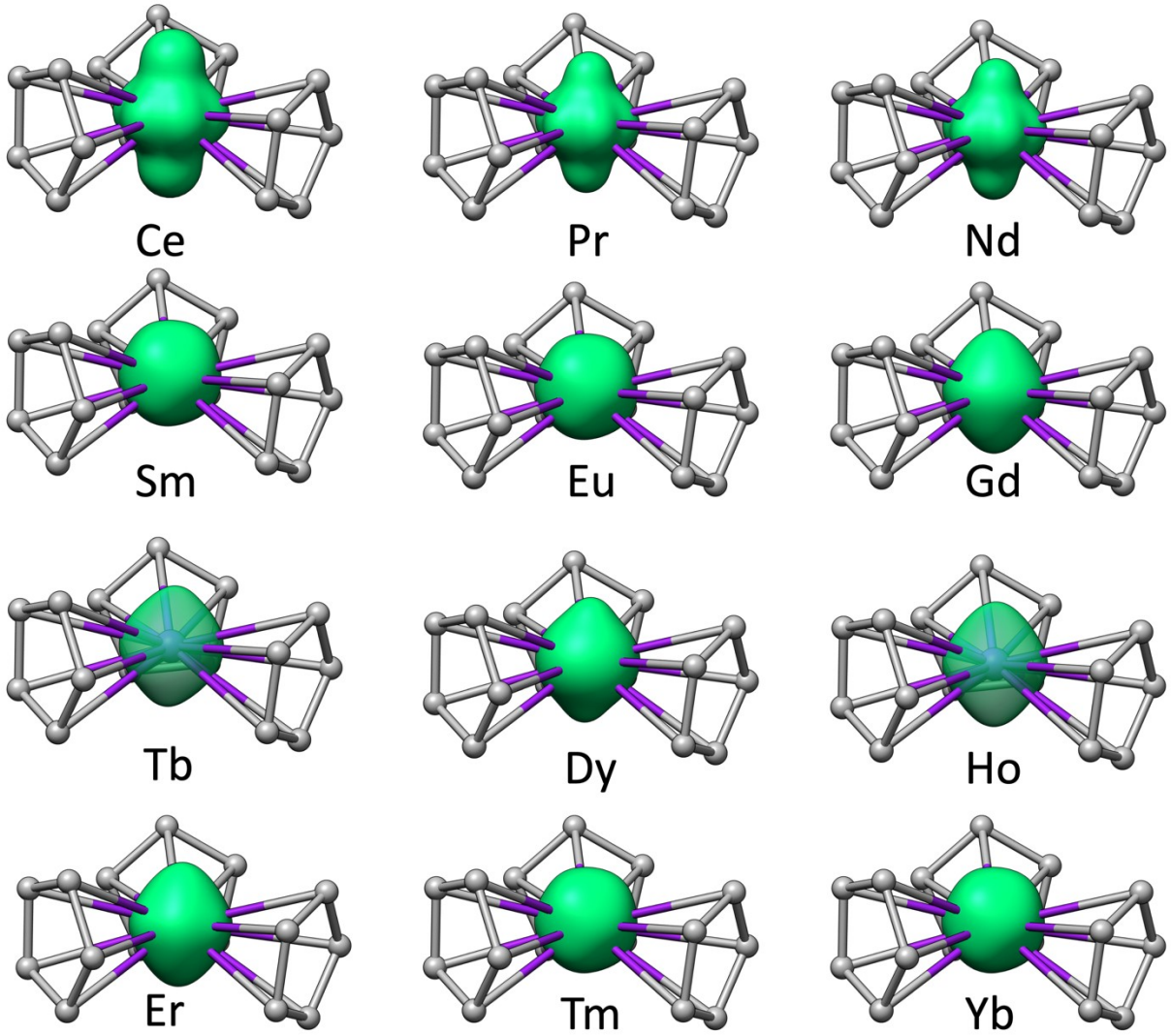

Figure S4. Ground state electron densities of the $[LnCp_3]^-$ complexes. This representation only considers the occupation numbers of the $4f + 5d_{z2}$ natural spin orbitals.

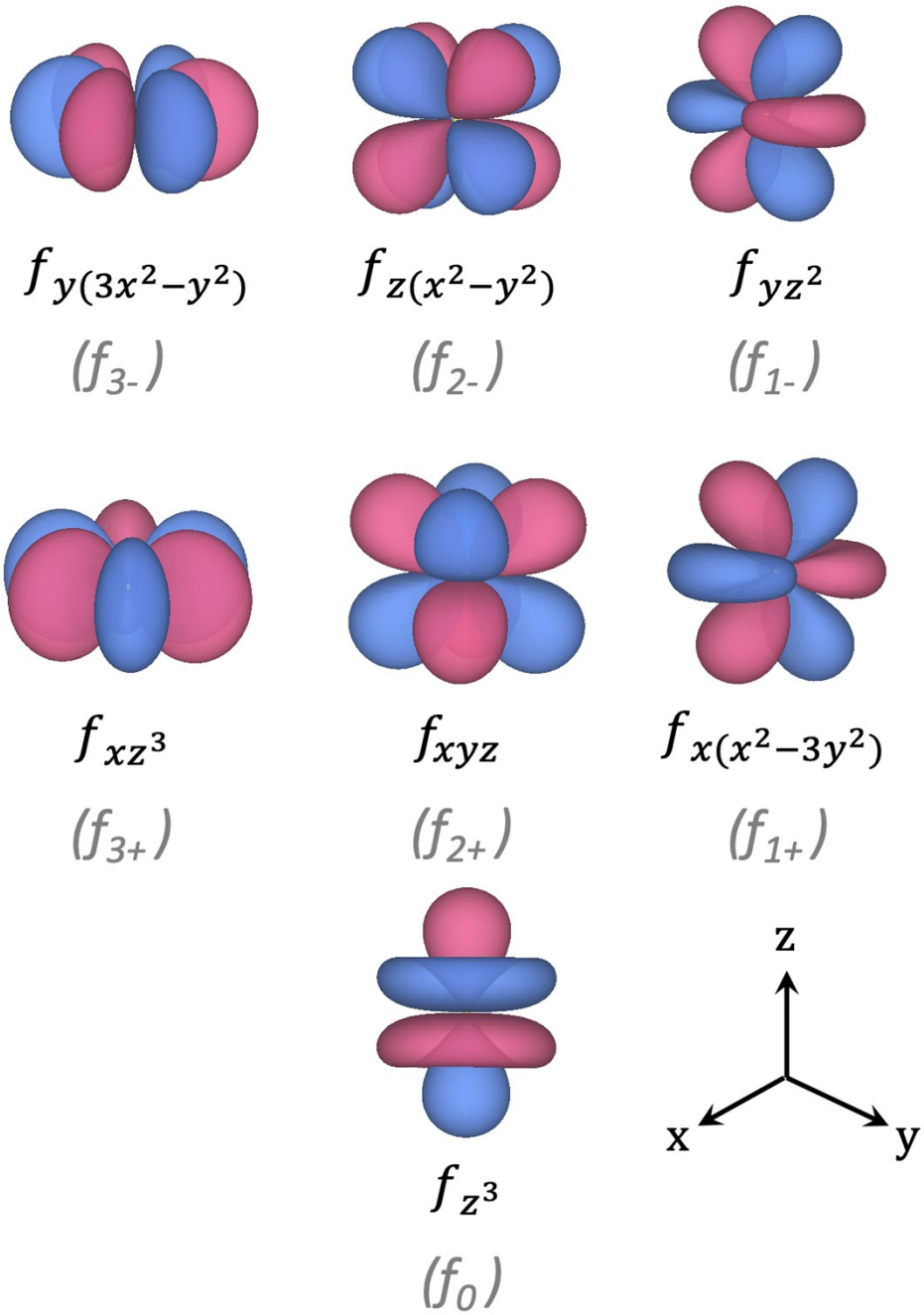

Figure S5. Depiction of the *f*-orbitals. Isosurface = 0.03.

References

1. MacDonald, M. R., Bates, J. E., Ziller, J. W., Furche, F. & Evans, W. J. Completing the Series of +2 Ions for the Lanthanide Elements: Synthesis of Molecular Complexes of Pr2+, Gd2+, Tb2+, and Lu2+. *J Am Chem Soc* **135**, 9857–9868 (2013).
2. MacDonald, M. R. *et al.* Expanding Rare-Earth Oxidation State Chemistry to Molecular Complexes of Holmium(II) and Erbium(II). *J Am Chem Soc* **134**, 8420–8423 (2012).
3. Fieser, M. E. *et al.* Structural, Spectroscopic, and Theoretical Comparison of Traditional vs Recently Discovered Ln2+ Ions in the [K(2.2.2-cryptand)][(C5H4SiMe3)3Ln] Complexes: The Variable Nature of Dy2+ and Nd2+. *J Am Chem Soc* **137**, 369–382 (2015).
4. ADF2019. Preprint at (2019).
5. Perdew, J. P., Burke, K. & Ernzerhof, M. Generalized Gradient Approximation Made Simple. *Phys Rev Lett* **77**, 3865–3868 (1996).
6. Van Lenthe, E. & Baerends, E. J. Optimized Slater-type basis sets for the elements 1–118. *J Comput Chem* **24**, 1142–1156 (2003).
7. Zhao, Y. & Truhlar, D. G. The M06 suite of density functionals for main group thermochemistry, thermochemical kinetics, noncovalent interactions, excited states, and transition elements: two new functionals and systematic testing of four M06-class functionals and 12 other functionals. *Theor Chem Acc* **120**, 215–241 (2008).
8. Anderson-Sanchez, L. M., Yu, J. M., Ziller, J. W., Furche, F. & Evans, W. J. Room-Temperature Stable Ln(II) Complexes Supported by 2,6-Diadamantyl Aryloxide Ligands. *Inorg Chem* **62**, 706–714 (2023).
9. Jenkins, T. F. *et al.* Tetramethylcyclopentadienyl Ligands Allow Isolation of Ln(II) Ions across the Lanthanide Series in [K(2.2.2-cryptand)][(C5Me4H)3Ln] Complexes. *Organometallics* **37**, 3863–3873 (2018).

10. Kundu, K. *et al.* A 9.2-GHz clock transition in a Lu(II) molecular spin qubit arising from a 3,467-MHz hyperfine interaction. *Nat Chem* **14**, 392–397 (2022).

11. Lenthe, E. van, Baerends, E. J. & Snijders, J. G. Relativistic regular two-component Hamiltonians. *J Chem Phys* **99**, 4597–4610 (1993).

12. Fleischauer, V. E. *et al.* Insight into the Electronic Structure of Formal Lanthanide(II) Complexes using Magnetic Circular Dichroism Spectroscopy. *Organometallics* **38**, 3124–3131 (2019).

13. Li Manni, G. *et al.* The OpenMolcas Web: A Community-Driven Approach to Advancing Computational Chemistry. *J Chem Theory Comput* **19**, 6933–6991 (2023).

14. Roos, B. O. *et al.* New Relativistic Atomic Natural Orbital Basis Sets for Lanthanide Atoms with Applications to the Ce Diatom and LuF3. *J Phys Chem A* **112**, 11431–11435 (2008).

15. Hess, B. A. Relativistic electronic-structure calculations employing a two-component no-pair formalism with external-field projection operators. *Phys Rev A (Coll Park)* **33**, 3742–3748 (1986).

16. Roos, B. O., Taylor, P. R. & Sigbahn, P. E. M. A complete active space SCF method (CASSCF) using a density matrix formulated super-CI approach. *Chem Phys* **48**, 157–173 (1980).

17. Malmqvist, P. Aake., Rendell, Alistair. & Roos, B. O. The restricted active space self-consistent-field method, implemented with a split graph unitary group approach. *J Phys Chem* **94**, 5477–5482 (1990).

18. Gagliardi, L. *et al.* Multiconfiguration Pair-Density Functional Theory: A New Way To Treat Strongly Correlated Systems. *Acc Chem Res* **50**, 66–73 (2017).

19. Malmqvist, P. Å., Roos, B. O. & Schimmelpfennig, B. The restricted active space (RAS) state interaction approach with spin–orbit coupling. *Chem Phys Lett* **357**, 230–240 (2002).

20. Barandiarán, Z. & Seijo, L. Radial correlation effects on interconfigurational excitations at the end of the lanthanide series: A restricted active space second order perturbation study of Yb2+ and SrCl2:Yb2+. *J Chem Phys* **138**, 074102 (2013).

21. Poe, T. N. *et al.* Influence of Outer-Sphere Anions on the Photoluminescence from Samarium(II) Crown Complexes. *Inorg Chem* **60**, 15196–15207 (2021).

22. Solís-Cespedes, E. & Páez-Hernández, D. Magnetic properties of organolanthanide(ii) complexes, from the electronic structure and the crystal field effect. *Dalton Trans.* **50**, 9787–9795 (2021).

23. Gendron, F. *et al.* Magnetic Properties and Electronic Structure of Neptunyl(VI) Complexes: Wavefunctions, Orbitals, and Crystal-Field Models. *Chem. - Eur. J*. **20**, 7994–8011 (2014).

24. Grimme, S., Antony, J., Ehrlich, S. & Krieg, H. A consistent and accurate ab initio parametrization of density functional dispersion correction (DFT-D) for the 94 elements H-Pu. *J Chem Phys* **132**, 154104 (2010).

25. Tang, J. & Zhang, P. *Lanthanide Single Molecule Magnets*. (Springer Berlin, Heidelberg, 2015).

26. Nugent, L. J. Chemical oxidation states of the lanthanides and actinides. in *Lanthanides and Actinides* vol. 7 195–219 (University Park Press, Baltimore, 1975).

27. Nugent, L. J., Baybarz, R. D., Burnett, J. L. & Ryan, J. L. Electron-transfer and f-d absorption bands of some lanthanide and actinide complexes and the standard (II-III) oxidation potential for each member of the lanthanide and actinide series. *J Phys Chem* **77**, 1528–1539 (1973).

28. Johnson, D. A. Relative stabilities of dipositive and tripositive lanthanoid ions in aqueous solution. *Journal of the Chemical Society, Dalton Trans.* 1671–1675 (1974) doi:10.1039/DT9740001671.

29. Mikheev, N. B. Lower oxidation states of lanthanides and actinides. *Inorganica Chim Acta* **94**, 241–248 (1984).

30. Mikheev, N. B. The lower oxidation states of the lanthanides and actinides in relation to the development of Mendeleev's Periodic Law. *Russ. J. Inorg. Chem* **29**, 258–263 (1984).

31. Mikheev, N. B. & Kamenskaya, A. N. Complex formation of the lanthanides and actinides in lower oxidation states. *Coord Chem Rev* **109**, 1–59 (1991).

32. Mikheev, N. B., Auerman, L. N., Rumer, I. A., Kamenskaya, A. N. & Kazakevich, M. Z. The anomalous stabilization of the oxidation state 2+ of lanthanides and actinides. *Russian Chemical Reviews* **76**, 827–841 (1992).

33. Kamenskaya, A. N. The lower oxidation state of the lanthanides in solution. *Russ. J. Inorg. Chem.* **29**, 251–258 (1984).

34. P Dorenbos. f → d transition energies of divalent lanthanides in inorganic compounds. *J. Phys.:Condens. Matter* **15**, 575 (2003).